

Spin-correlation coefficients and phase-shift analysis for $p + {}^3\text{He}$ elastic scattering

T. V. Daniels,* C. W. Arnold, J. M. Cesaratto, T. B. Clegg, A. H. Couture, H. J. Karwowski, and T. Katabuchi†

*The University of North Carolina at Chapel Hill, Chapel Hill, North Carolina 27599-3255, USA and**Triangle Universities Nuclear Laboratory, Durham, North Carolina 27708-0308, USA*

(Received 30 March 2010; published 10 September 2010)

Angular distributions for the target spin-dependent observables A_{0y} , A_{xx} , and A_{yy} have been measured using polarized proton beams at several energies between 2 and 6 MeV and a spin-exchange optical pumping polarized ${}^3\text{He}$ target. These measurements have been included in a global phase-shift analysis following that of E. A. George and L. D. Knutson [*Phys. Rev. C* **67**, 027001 (2003)], who reported two best-fit phase-shift solutions to the previous global $p + {}^3\text{He}$ elastic-scattering database below 12 MeV. These new measurements, along with measurements of cross-section and beam-analyzing power made over a similar energy range by B. M. Fisher *et al.* [*Phys. Rev. C* **74**, 034001 (2006)], allowed a single, unique solution to be obtained. The new measurements and phase shifts are compared with theoretical calculations using realistic nucleon-nucleon potential models.

DOI: [10.1103/PhysRevC.82.034002](https://doi.org/10.1103/PhysRevC.82.034002)

PACS number(s): 21.45.-v, 21.30.-x, 24.70.+s, 25.40.Cm

I. INTRODUCTION

Beginning from the picture that atomic nuclei are composed of interacting nucleons, *ab initio* calculations of light nuclear systems are based on realistic nucleon-nucleon potential models, which have been adjusted to reproduce two-nucleon (NN) scattering and bound-state data accurately [1]. This effort has included calculations of low-energy scattering observables for the three-nucleon ($3N$) and four-nucleon ($4N$) systems. The latter calculations are especially significant because the $4N$ system is the lightest to exhibit thresholds and resonances [2]; so its correct description is an important milestone for this approach.

The comparison of *ab initio* calculations with nucleon-deuteron-scattering measurements reveals general agreement for the cross section and tensor analyzing powers, but significant underprediction of the beam and target analyzing powers [3]. A similar “ A_y puzzle” has been reported for $p + {}^3\text{He}$ elastic scattering [4]. All NN models and theoretical methods yield this disagreement, which is not resolved by including the $3N$ force necessary to reproduce the $3N$ and $4N$ binding energies [5].

The study of this discrepancy may benefit from the more thorough comparison between theory and experiment made possible by a set of experimental phase shifts and mixing parameters. For example, A_y is known to be particularly sensitive to the splitting between triplet P -wave phase shifts [4]. A wealth of experimental data exists for $p + {}^3\text{He}$ elastic scattering below 12 MeV proton energy, with the most recent phase-shift analysis by George and Knutson [6] performed on a database of over 1000 data points. That analysis, however, was unable to constrain a unique set of parameters and instead obtained two solutions which fit the data equally

well. The difference between the two solutions was largest for spin-correlation coefficients below 4 MeV, where no such data exist. With the aim of resolving the phase-shift ambiguity, we have used a polarized ${}^3\text{He}$ target [7] to measure angular distributions of the spin-correlation coefficients A_{xx} and A_{yy} at proton energies between 2 and 6 MeV and included those new data, along with those of Fisher *et al.* [4], in a new global phase-shift analysis following that of George and Knutson [6].

II. EXPERIMENT**A. Polarized target**

Polarized and unpolarized beams from the Triangle Universities Nuclear Laboratory (TUNL) tandem accelerator were directed by an analyzing magnet to a 62-cm-diameter scattering chamber. The polarized ${}^3\text{He}$ target was specifically designed for low-energy charged-particle-scattering experiments and has been described previously in detail [7]. In contrast to previous targets used for the same purpose [8–13] that operated by metastability-exchange optical pumping (MEOP), the present target used spin-exchange optical pumping (SEOP). This method has previously been used in polarized ${}^3\text{He}$ targets for electron-scattering [14] and γ -ray-scattering [15] experiments.

The primary advantage of SEOP over MEOP is greater target thickness, since it polarizes ${}^3\text{He}$ at a pressure of about 8 bar instead of several mbar. The need to minimize energy loss for the incident and scattered particles for the low-energy application, however, required the use of thin windows to contain the gas. Since such windows cannot withstand the full 8-bar ${}^3\text{He}$ pressure, we optically pumped ${}^3\text{He}$ in a system separate from the scattering target cell. The target cell was then batch-filled with polarized gas to a pressure of approximately 1 bar.

The target cell was a 5.1-cm Pyrex sphere with openings along the equator for the incident and scattered particles. These were covered with 7.6- μm Kapton foil affixed with Torr Seal epoxy [16]. The cell was housed in a compact sine- θ coil to provide a uniform 0.7-mT magnetic holding field. An NMR

*tvdaniels@physics.umass.edu; Present address: Department of Physics, University of Massachusetts, Amherst, MA 01003.

†Present address: Research Laboratory for Nuclear Reactors, Tokyo Institute of Technology, Ookayama, Meguro-ku, Tokyo 152-8550, Japan.

coil pressed against the rear of the cell was used to measure the target polarization, as discussed below.

The ^3He polarization was produced by SEOP using Rb as the intermediate alkali metal. A 60-W fiber-coupled diode laser system tuned to the 795-nm Rb D1 absorption line provided, with appropriate optics, the circularly polarized light for the optical pumping. Two modifications to our original polarizer [7] were attempted. In agreement with results reported by others [17], the use of “mixed-metal” optical pumping cells containing both Rb and K was found to decrease the “spin-up” time [18]. In this work, the typical time required to reach saturation polarization was about 12 h with mixed-metal cells, compared to about 24 h using only Rb.

The other modification was the use of frequency-narrowed laser light for optical pumping. Following the work of B. Chann *et al.* [19], an external Littrow cavity was constructed and used to reduce the output width of a 50-W diode bar array from 2 to 0.3 nm [20]. The narrowed output power was about 30 W. Unfortunately, the ^3He polarization produced with this laser system was not consistently higher than that produced with the 60- to 80-W broadband system, perhaps because more light was absorbed from the latter. The majority of the present data was therefore taken with the broadband laser.

B. Scattering measurements

The experimental arrangement is illustrated in Fig. 1. Beam current on the target cell was limited to 50 nA to minimize damage to the Kapton foils. Failure of the epoxy, especially that sealing the beam-exit foil, caused cells to leak after a few days. Each such failure required a cell change and recalibration of the NMR signal (see below).

Measurements were made at five proton energies below 6 MeV that overlap the energies of both Fisher *et al.* [4] and Alley and Knutson [13]. Analyzing magnet settings that determined the beam energy were selected according to the calibration of Ref. [21]. Beam energies were adjusted to offset energy loss in the foils and gas, as modeled with the computer program SRIM [22]. Bombarding energies for data taken with different thickness entrance foils were slightly different, and the error-weighted average value was adopted. The uncertainty in SRIM stopping powers for materials used was estimated by comparison with experimental stopping powers [22] and ranged from 3% to 10%. An uncertainty of 10% was assigned

to cases where no data were present in the relevant energy range.

The beam and target polarizations were reversed frequently during data taking. The beam polarization was reversed at either 1 or 10 Hz in the sequence “uddduud,” where “u” means “spin-up” and “d” means “spin-down.” The target polarization was reversed less frequently, since a few seconds were required to reverse the target’s magnetic field. Polarized target data were collected for intervals of 2.5 m in each spin orientation, with NMR measurements of the magnitude of the polarization made immediately before and after the orientation was reversed. The target polarization decayed with a 2- to 3-h time constant, so this process was stopped when the gas was judged to be too depolarized, generally after about 1 h. At that time the gas was exhausted from the target cell, which was then flushed with research-grade N_2 and refilled with a new batch of polarized gas. The recovered depolarized ^3He gas was circulated through a LN_2 -cooled trap to remove impurities before repolarization.

Scattered particles emerging from the target were detected by four pairs of Si detectors that could be rotated to the desired angle. Available angles were restricted by the windows in the sine- θ coil’s μ -metal shield to 20° increments between 30° and 150° . The shield could be moved axially so that “intermediate” angles offset by 10° were also available. The detectors were each placed in an Al holder behind two brass collimators spaced 5.08 cm apart in an Al “snout,” which restricted the range of scattering angles visible to the detector to 1.5° . Detectors were as close as possible to the target without the 30° snout’s touching the sine- θ coil, so that the distance from the center of the target cell to the front collimators was about 10.2 cm. Beam current on target was measured by an electrostatically suppressed Faraday cup located about 0.5 m behind the target cell. The charge went to ground through a current integrator to measure the relative number of beam particles in each spin state.

An example detector spectrum is shown in Fig. 2. The peaks corresponding to protons elastically scattered from ^3He and small amounts of N_2 were well separated. The latter was required by the optical pumping process [7]. Occasionally ^4He was added to the cell to measure the beam polarization, and in some cases that peak overlapped the ^3He peak. In such cases the peaks were fit with skewed Gaussians. A pulser was added

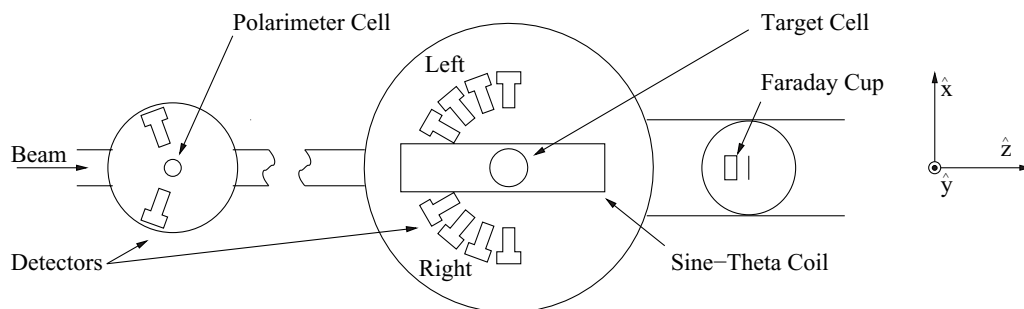
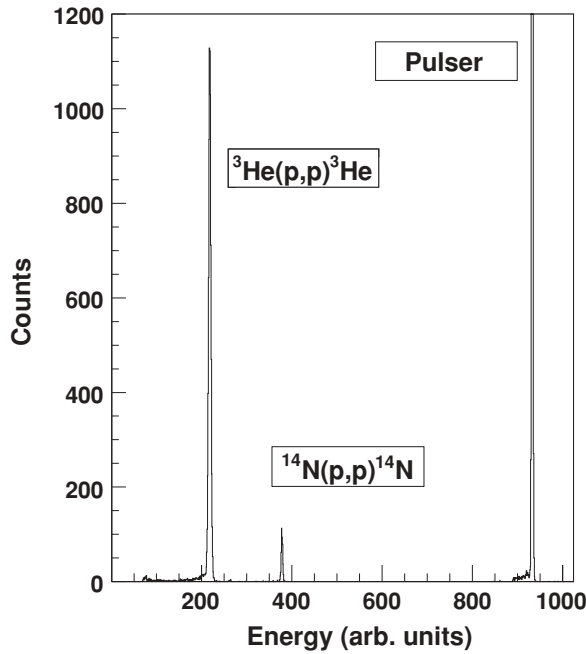


FIG. 1. Diagram of the experimental arrangement. The polarimeter chamber at left was used with the detectors either horizontal, as shown, or vertical. The polarimeter cell was removed from the beam during data taking to allow the beam to reach the target chamber. The coordinate system used to define the scattering observables is also shown.


 FIG. 2. ${}^3\text{He}(p,p){}^3\text{He}$ spectrum taken at 5.54 MeV and 90° .

to each spectrum to measure electronic dead time, which was typically less than 1%.

The observables were extracted from peak yields in left (L) and right (R) detectors using an extension of the geometrical mean method [23] for analyzing powers to include polarized beam and target. With the spins aligned vertically along the $\pm y$ axis, the following cross ratios were formed:

$$X_1 = \sqrt{\left(\frac{L\uparrow\uparrow + L\uparrow\downarrow}{L\downarrow\uparrow + L\downarrow\downarrow}\right) \left(\frac{R\downarrow\uparrow + R\downarrow\downarrow}{R\uparrow\uparrow + R\uparrow\downarrow}\right)} = \frac{1 + p_y A_{y0}}{1 - p_y A_{y0}},$$

$$X_2 = \sqrt{\left(\frac{L\uparrow\uparrow + L\downarrow\uparrow}{L\uparrow\downarrow + L\downarrow\downarrow}\right) \left(\frac{R\uparrow\downarrow + R\downarrow\downarrow}{R\uparrow\uparrow + R\downarrow\uparrow}\right)} = \frac{1 + p_y^T A_{0y}}{1 - p_y^T A_{0y}},$$

$$X_3 = \sqrt{\left(\frac{L\uparrow\uparrow + L\downarrow\downarrow}{L\uparrow\downarrow + L\downarrow\uparrow}\right) \left(\frac{R\uparrow\uparrow + R\downarrow\downarrow}{R\uparrow\downarrow + R\downarrow\uparrow}\right)} = \frac{1 + p_y p_y^T A_{yy}}{1 - p_y p_y^T A_{yy}},$$

where the arrows indicate the beam and target spin state; for example, $L\uparrow\downarrow$ refers to the number of particles scattered into the left detector while the beam was spin-up and the target was spin-down. The detector yields were normalized to the current integration and target pressure, which was known to about 2%, for each spin state. The polarization of the beam and target are given by p and p^T , respectively. The observables are, therefore,

$$A_{y0} = \frac{1}{p_y} \left(\frac{X_1 - 1}{X_1 + 1} \right), \quad (1)$$

$$A_{0y} = \frac{1}{p_y^T} \left(\frac{X_2 - 1}{X_2 + 1} \right), \quad (2)$$

$$A_{yy} = \frac{1}{p_y p_y^T} \left(\frac{X_3 - 1}{X_3 + 1} \right), \quad (3)$$

where the quantity in parentheses is the measured scattering asymmetry. Similarly, when the beam and target spins are

aligned horizontally along the x axis,

$$A_{xx} = \frac{1}{p_x p_x^T} \left(\frac{X_3 - 1}{X_3 + 1} \right). \quad (4)$$

If either the beam or the target is unpolarized, only one analyzing power will be nonzero, and its expression reduces to the usual cross ratio for analyzing powers,

$$A_y = \frac{1}{p} \frac{\sqrt{\frac{L\uparrow R\downarrow}{L\downarrow R\uparrow}} - 1}{\sqrt{\frac{L\uparrow R\downarrow}{L\downarrow R\uparrow}} + 1}, \quad (5)$$

where p refers to the nonzero polarization. The same is true for the scattering of spin-1/2 protons from spin-0 α particles used for beam polarimetry.

C. Beam polarimetry

A proton beam leaving an atomic beam polarized ion source [24] passed through a calibrated Wien filter at the ion source to orient the spin quantization axis of the beam in the desired direction at the scattering chambers. The magnitude of the beam polarization was measured periodically using $p + {}^4\text{He}$ elastic scattering in either the target cell or a separate cell in a polarimeter chamber installed upstream of the target chamber. Detectors in the latter could be mounted at 110° in the horizontal or vertical scattering planes, so that either polarization component could be measured. The cell in the polarimeter chamber could be moved to insert it periodically into the beam for polarization measurements.

The $p + {}^4\text{He}$ asymmetries were divided by the analyzing power A_y to obtain the beam polarization. Published phase shifts [25] were used in a spin-1/2-on-spin-0 phase-shift code to calculate the analyzing powers for the energies at the center of the cell as determined from SRIM. The uncertainty in the resulting analyzing power was typically 2%.

For more than half of the spin-correlation data, however, the beam polarization was unstable, so that periodic monitoring did not necessarily determine the average polarization. Therefore, the beam polarization for all A_{yy} measurements was determined by normalizing our relative A_{y0} measurements to published values [13,21]. Each point in a relative A_{y0} angle set was divided by a value linearly interpolated from those previous measurements at the same energy, and the polarization was taken to be the average of these ratios. An uncertainty of 0.02 was assigned to the polarization and added in quadrature with statistical uncertainties. No published data were available at 2.7 MeV; therefore, smooth curves were fit through existing distributions at each angle vs energy and evaluated at 2.7 MeV. The normalization then proceeded as described previously.

The procedure was extended to about one-third of the A_{xx} measurements by ‘‘tipping’’ the spin 20° out of the plane with the Wien filter and applying the aforementioned analysis to the y component. The x component of the beam polarization was obtained by multiplying the y component by the ratio of the two components. An 8% normalization uncertainty was applied to those angular distributions to account for the estimated 1.5° uncertainty in the relative azimuthal orientation

of the scattering plane and the polarized beam's quantization axis. The remaining A_{xx} measurements with stable beam polarization relied on polarimeter measurements as described previously.

D. Target polarimetry

As discussed in detail by Katabuchi *et al.* [7], the target polarization was monitored using pulsed NMR. Briefly, an rf pulse at the Larmor frequency set by the sine- θ coil magnetic field was sent through a small coil pressed against the rear of the target cell. The resulting collective precession of ^3He spins about that magnetic field induced a signal proportional to both the ^3He polarization and the pressure. This voltage was then divided by the cell pressure to give a relative measure of polarization.

These relative NMR data for each target cell were calibrated against separate $^4\text{He} + ^3\text{He}$ A_y measurements at an energy and angle where $A_y = -1$. The resulting scattering asymmetries for an incident ^4He beam, given by Eq. (5), were therefore direct measurements of the ^3He target polarization. This calibration method was motivated by the prediction of Plattner and Bacher [26] of an $A_y = -1$ extremum near 15.33 MeV ^3He laboratory energy and a 47° ^3He laboratory scattering angle. Their prediction for its location was only approximate. Thus, *relative* measurements of A_y in $^4\text{He} + ^3\text{He}$ elastic scattering as a function of angle and energy near the predicted extremum were made to define the local minimum. We determined θ_{\min} to be $46.64 \pm 0.22^\circ$, and the measurements of A_y vs energy agree with the prediction of D. M. Hardy *et al.* [27,28] of a very broad minimum.

The simultaneous NMR scattering calibrations for various target cells were made at 45° and E_α between 15.44 and 15.82 MeV. Because this was not exactly the minimum point for A_y , a target polarization value was assigned from the relative measurements with an uncertainty of 3%, normalized so that the minimum A_y was equal to -1 .

E. Steering effect

The target magnetic field, though small, steered the incoming and scattered protons slightly through the Lorentz force, as sketched in Fig. 3. When the B field was reversed to reverse the target spin, the particles were steered oppositely, and the relationship between detector yields was reversed.

First, the incoming beam deflection moved the scattering center closer to one detector and further from the other, thus changing their relative solid angles. Second, the scattered protons were deflected to emerge from the target cell at angles slightly different than those at which they were actually scattered. Thus, for a given orientation of the magnetic field, the actual scattering angle of particles reaching one detector of a left/right pair was more forward than the detector angle, while that of those reaching the other detector was more backward. This difference in scattering angle produced an instrumental asymmetry through the angular dependence of the differential cross section. These two steering effects, unlike other systematic effects [29], produced systematic instrumental asymmetries that were *not* canceled by reversing the target spin.

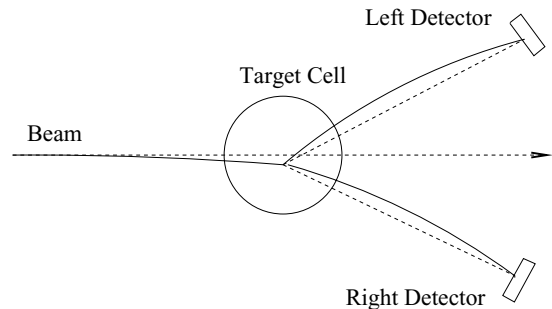


FIG. 3. Steering of the incoming proton beam and scattered particles by the sine- θ coil's magnetic field. The target cell and detectors are shown from above. The beam is incident from the left on the gas cell along the dotted line, but deflected as shown by the magnetic field, which is oriented out of the page. Similarly, the scattered particles travel along curved paths to the detectors. The figure is not to scale, and the size of the effect is exaggerated for clarity.

These effects were largest at our lowest bombarding energies. Figure 4 shows the target-scattering asymmetry, as defined for Eq. (2), measured while the target was unpolarized, when the asymmetries corresponding to the target analyzing power and spin-correlation coefficients should be zero. While this was true for measurements with the sine- θ coil's magnetic field turned off, nonzero asymmetries were obtained with the field on. The asymmetries for A_{yy} and A_{xx} (not pictured), however, were consistent with zero whether the field was on or off. This difference between the target and spin-correlation asymmetries is to be expected, since the expression for X_2 , which appears in Eq. (2), involves detector yields from one target magnetic field orientation in the numerator and the other in the denominator, while that for X_3 , which appears in Eqs. (3) and (4), involves both target spin states in both the numerator and the denominator and so tends to average out effects that depend only on the target magnetic field.

The result of a simple calculation of these two effects at 2.25 MeV is also shown in Fig. 4. Though the largest deflection angle calculated was 0.1° , the resulting asymmetries are large enough to interfere with polarized target measurements. The

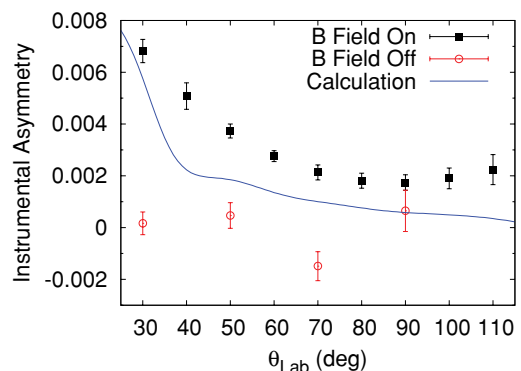


FIG. 4. (Color online) Instrumental target asymmetries measured at 2.25 MeV with the sine- θ coil's magnetic field both on and off. A simple calculation of the effect of magnetic steering that ignores the finite size of the beam and target is also shown.

calculation neglects the finite size of the beam and target and simply determines the energy loss, modeled in SRIM, and magnetic steering of incoming and scattered protons in small steps as they proceed through the magnetic field. The calculation reproduces the general size and forward-angle trend of the effect, but with insufficient detail to be used to correct the data.

Rather than pursue more complex calculations that correctly include the finite beam and target sizes, actual measurements of these instrumental asymmetries, obtained both from direct measurements with unpolarized ^3He and by extrapolating polarized target asymmetries to zero polarization, were subtracted from polarized target A_{0y} data. The corrections obtained in this way were often large, being several times the size of the observable at forward angles at the lowest proton energies.

F. Results for observables

The present measurements of A_{0y} , A_{yy} , and A_{xx} are shown in Figs. 5–7. Each plot also includes a curve calculated from the new best-fit effective-range parameters of the global phase-shift analysis (PSA) discussed later in this article, as well as previous measurements where available. The overall agreement with the previous measurements is good, with the most forward-angle A_{yy} points of Alley and Knutson [13] at 5.54 MeV being the only exception, and the present results have smaller error bars. The new measurements are well fit by the phase-shift analysis, except for the two most-forward-angle A_{0y} points at 3.15 and 4.02 MeV. The forward-angle points required the largest correction for magnetic steering, so the disagreement with the PSA may indicate that the correction applied to those points was not sufficiently accurate.

III. PHASE-SHIFT ANALYSIS

A phase-shift analysis of the global $p + ^3\text{He}$ elastic-scattering database below $E_p = 12$ MeV was performed following the earlier work of George and Knutson [6], with the addition of about 300 new data points, including the $d\sigma/d\Omega$ and A_{y0} measurements of Fisher *et al.* [4] and the present A_{0y} , A_{yy} , and A_{xx} measurements. These additional data all fell between 1.0 and 5.54 MeV. The search routine was the same as that used in the previous analysis and was provided by George [31].

The program calculated scattering observables as functions of scattering matrix elements, which were in turn parametrized using phase shifts and mixing parameters according to the Blatt-Biedenharn convention [32]. The phase shifts and mixing parameters used were 1S_0 , 3S_1 , 1P_0 , 3P_2 , 3P_1 , 3P_0 , 1D_2 , $\epsilon(1^-)$, $\epsilon(1^+)$, and $\epsilon(2^-)$, as well as consolidated 3D_j and 3F_j triplet phase-shifts. The energy dependence of the phase shifts and mixing parameters was described by the first three terms in a modified effective-range expansion. These 36 effective-range parameters were adjusted to minimize χ^2 with respect to the experimental database using the MINUIT package [33]. As described in Ref. [6], the database was broken into groups of measurements thought to have common normalizations.

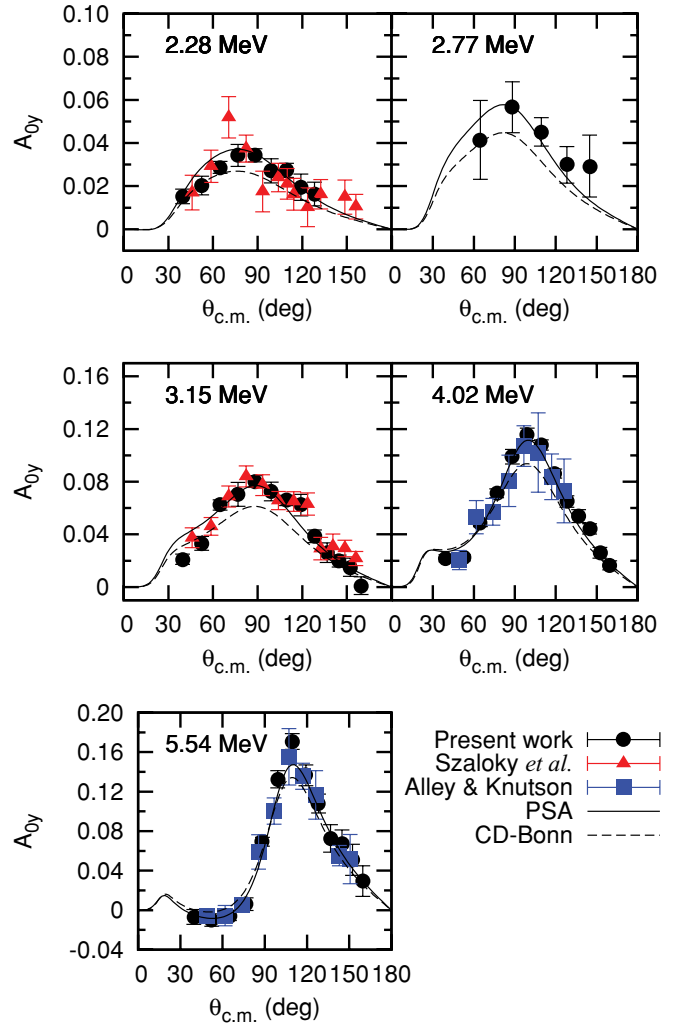


FIG. 5. (Color online) Present measurements of A_{0y} at five proton beam energies, together with the global PSA fit. Measurements of Szaloky and Seiler [30] and Alley and Knutson [13] as well as theoretical calculations of Deltuva and Fonseca [36] using the CD-Bonn potential [37] are also shown.

These 21 normalization factors were analytically adjusted at each step of the parameter search to further minimize χ^2 .

Initial parameter searches resulted in multiple solutions that were discontinuous in one or more of the 1D_2 , 3D_j , and 3F_j phase shifts. The discontinuity, discussed also by Alley [34], occurred when the phase shift crossed zero and was deemed unphysical. The number of such solutions was reduced by fixing the small 3F_j phase shift at the values obtained using the database of Alley and Knutson [13]. The best-fit χ^2 when this parameter was not searched increased by only 0.2%. All but one of the remaining solutions, which spanned a range of about 10% in χ^2 , were rejected by demanding that the phase shifts be continuous in the energy range covered by the database. The remaining solution, which has the lowest χ^2 and is adopted as the present global result, yields a small positive scattering length for 3D_j , indicating that a discontinuity must occur in that phase at an energy below the lower end of the database (100 keV). The best-fit effective range

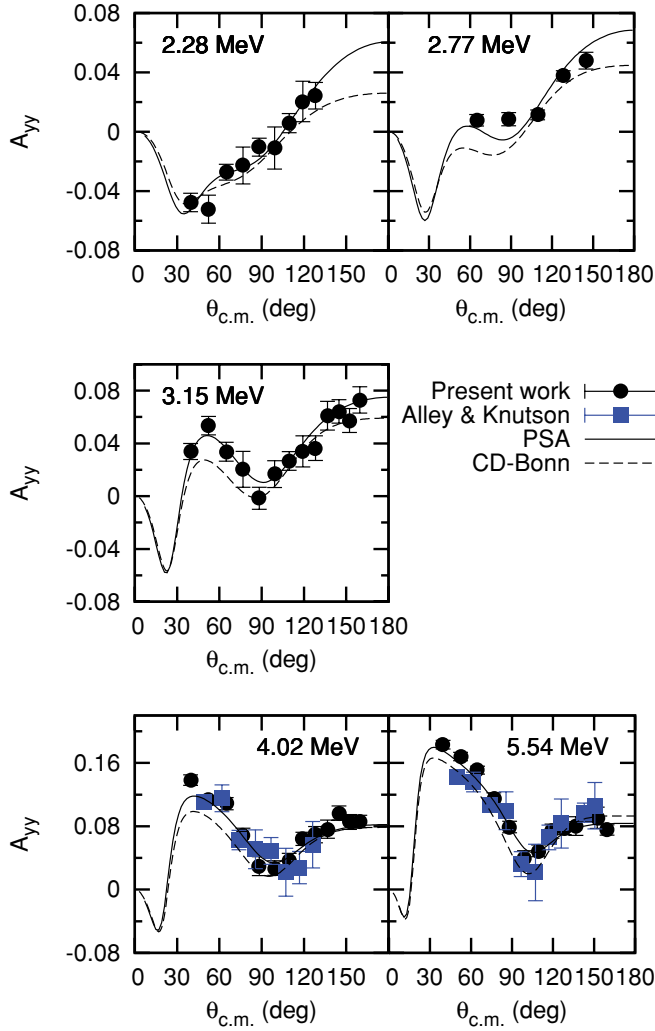


FIG. 6. (Color online) Present measurements of A_{yy} at five proton beam energies, together with other results as mentioned for Fig. 5.

parameters and associated statistical uncertainties are given in Table I.

The global solution had a χ^2 per datum of about 2 for the data added in this analysis. This could be improved to between 1.3 and 1.5 if points whose individual χ^2 contributions exceeded 10 were rejected. About half of these 13 out of about 300 new points seemed simply to be random outliers, while the others seemed to be associated with systematic problems. These included some forward-angle A_{0y} points that had been corrected for magnetic steering. Another apparent systematic problem was found for A_{y0} data at 1.60 MeV for which the four most-forward-angle points disagreed with the phase-shift analysis. The effect of their removal on the phase shifts was generally negligible, and in all cases within the range of systematic error indicated by the single-energy analyses described later.

To gauge the effects of systematic errors, single-energy analyses were performed at energies where new spin-correlation and new or existing cross-section measurements were available, that is, at nominal proton energies of 2.25, 3.13, 4.00, and 5.54 MeV. All measurements within 100 keV of the

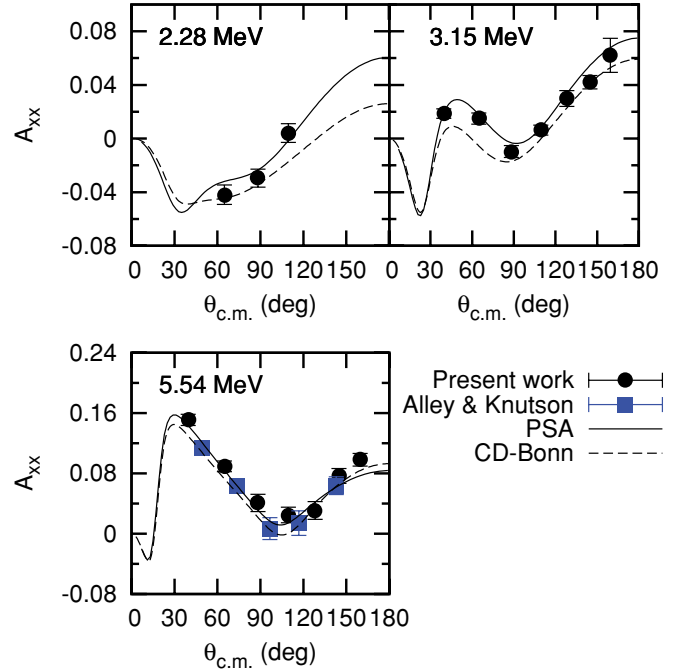


FIG. 7. (Color online) Present measurements of A_{xx} at three proton beam energies, together with other results as mentioned for Fig. 5.

nominal energies were included. The same method was used for these single-energy fits as for the energy-dependent work, except that the phase shifts were searched directly, instead of through the effective-range parameters.

The present phase-shift results, both single-energy and global, are shown in Fig. 8, along with those of Refs. [35] and [6]. The addition of the new data removes the S -wave ambiguity in the latter results without qualitatively modifying the behavior of the other parameters, such as the resonant P -wave behavior associated with excited states of ${}^4\text{Li}$. The new, low-energy data also seem to introduce some tension with previous, higher-energy data, as indicated by differences between the present global results and those of Ref. [35] for 1S_0 and 3P_0 .

TABLE I. Best-fit effective-range parameters with statistical uncertainties.

Phase	$a_0 \times 10^{-2}$	$a_1 \times 10^{-1}$	a_2
1S_0	-9.0 ± 0.4	7.9 ± 0.6	1.0 ± 0.2
3S_1	-11.06 ± 0.17	7.5 ± 0.3	-0.09 ± 0.08
1P_1	5.44 ± 0.15	-1.7 ± 0.3	4.05 ± 0.13
3P_2	2.128 ± 0.012	1.591 ± 0.018	0.356 ± 0.009
3P_1	1.63 ± 0.02	2.06 ± 0.04	0.592 ± 0.018
3P_0	8.8 ± 0.3	-1.5 ± 0.3	2.40 ± 0.09
1D_2	-14 ± 4	15 ± 4	-8.3 ± 1.3
3D_j	-0.06 ± 0.19	-3.4 ± 0.9	7.2 ± 0.4
3F_j	4.19	38.3	-6.29
$\epsilon(1^+)$	-5 ± 5	34 ± 6	-10.7 ± 1.7
$\epsilon(1^-)$	-420 ± 11	230 ± 10	-41 ± 2
$\epsilon(2^-)$	17 ± 7	8 ± 6	-5.9 ± 1.4

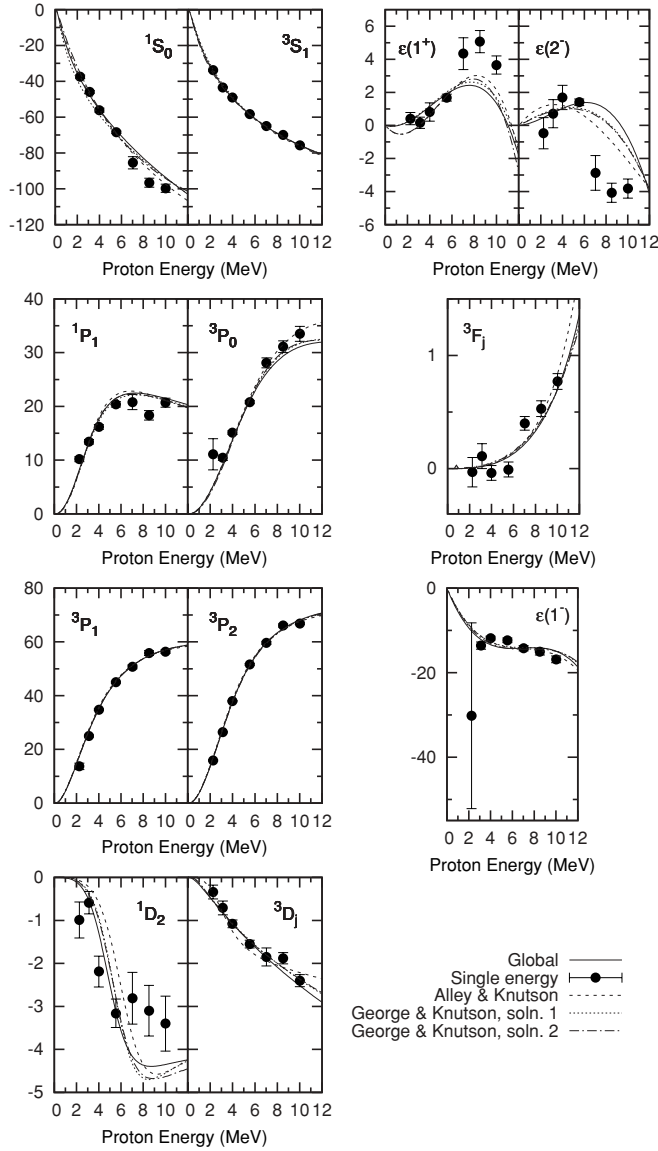


FIG. 8. Phase-shift results, in degrees, as functions of proton laboratory energy in MeV. Both the global and single-energy results of this analysis are shown, as well as the previous results of Alley and Knutson [35] and George and Knutson [6].

Results for selected phase shifts, in degrees, are tabulated in Tables II and III at the nominal energies of the single-energy analyses. The quoted uncertainties include statistical uncertainties and systematic sources including differences between the single-energy and global analyses and variation of the parameters when outliers are excluded. Theoretical calculations, described in the next section, using the CD-Bonn realistic NN potential are also shown for comparison.

IV. COMPARISON WITH THEORETICAL CALCULATIONS

We first compare our new experimental results with recent *ab initio* momentum-space calculations from Deltuva and Fonseca [36] that rigorously include the Coloumb interaction and use a variety of $2N$ potentials. For simplicity, only

TABLE II. Global phase-shift analysis results at 2.25 and 3.15 MeV.

Phase	2.25 MeV		3.15 MeV	
	Present	CD-Bonn	Present	CD-Bonn
1S_0	-39.1 ± 1.7	-39.6	-48.7 ± 0.9	-49.3
3S_1	-34.5 ± 0.7	-34.8	-42.90 ± 0.09	-42.9
1P_1	8 ± 2	10.6	13.4 ± 0.4	14.9
3P_0	5 ± 6	7.9	9.7 ± 0.8	12.3
3P_1	17 ± 4	16.9	27.0 ± 1.9	26.1
3P_2	16.5 ± 0.7	16.0	27.7 ± 1.2	25.8
$\epsilon(1^-)$	-10 ± 20	-8.9	-12.2 ± 1.7	-8.3

their results obtained using the CD-Bonn potential [37] are shown in Figures 5–7, but the results of the other realistic $2N$ potentials considered, AV18 [38] and N3LO, which is derived from chiral perturbation theory at next-to-next-to-next-to-leading order [39], are similar. The A_{y0} calculations consistently underpredict the new results by 10%–20% at the maximum. This is similar to, though smaller than, the previously established 40% underprediction of A_{y0} by several realistic potentials and theoretical methods [4,36].

The theoretical results for the spin-correlation coefficients at $E_p = 2.77$ MeV and above agree with the present results at backward angles but are too small by about 0.02 at forward angles. The disagreement for backward angles between the theoretical results and the present phase-shift analysis at 2.28 MeV may result from the lack of back-angle data points, especially for A_{xx} .

For the phase shifts, the theoretical S waves generally agree well with the present results, while the theoretical 1P_1 and 3P_0 phase shifts are larger. The theoretical 3P_1 and 3P_2 phase shifts, as well as the $\epsilon(1^-)$ mixing parameter, are consistently smaller than our present results. The splitting between the triplet P waves is also underpredicted, as shown in Fig. 9, where $\delta = ^3P_2 - (^3P_1 + ^3P_0)/2$. This is interesting in light of the strong dependence of A_{y0} on that splitting [4].

Results from Deltuva and Fonseca [36] using the Doleschall potential INOY04 [40] are also shown in Figs. 9 and 10. That potential introduces nonlocalities to simulate implicitly the effect of three-nucleon forces, which are necessary to reproduce three- and four-nucleon binding energies. The parameters of those nonlocalities are adjusted to reproduce $3N$ scattering

TABLE III. Global phase-shift analysis results at 4.00 and 5.55 MeV.

Phase	4.00 MeV		5.55 MeV	
	Present	CD-Bonn	Present	CD-Bonn
1S_0	-56.3 ± 0.6	-56.8	-67.8 ± 0.9	-67.1
3S_1	-49.3 ± 0.5	-49.7	-58.6 ± 0.3	-59.2
1P_1	17.3 ± 1.6	18.2	21.2 ± 1.7	22.5
3P_0	14.1 ± 0.9	16.6	21.3 ± 0.7	23.9
3P_1	34.9 ± 0.3	33.9	45.2 ± 0.5	43.0
3P_2	37.6 ± 0.6	34.9	51.5 ± 0.5	47.0
$\epsilon(1^-)$	-13 ± 2	-9.0	-14 ± 2	-9.6

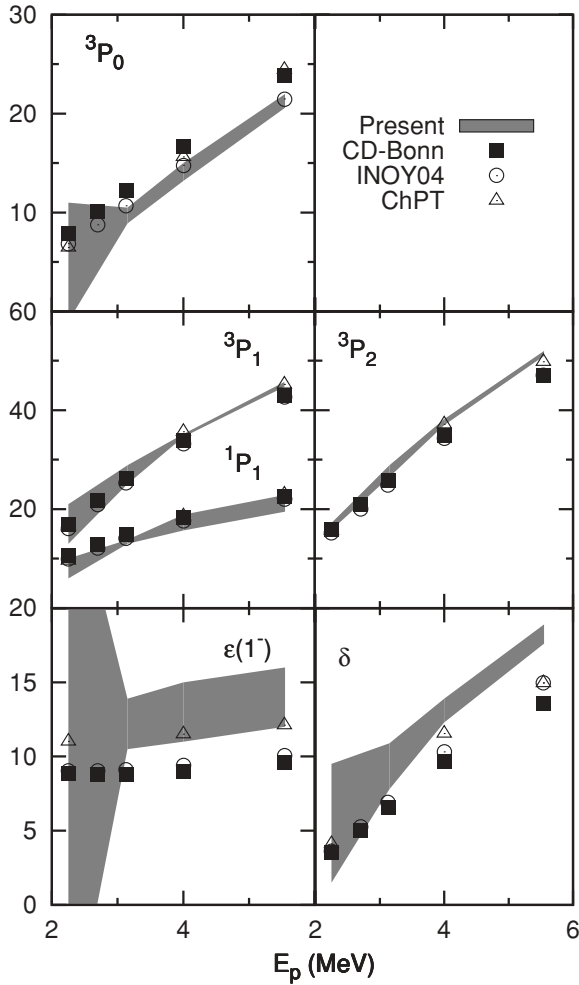


FIG. 9. Comparison of the present P -wave phase shifts, in degrees, with the theoretical results of Deltuva and Fonseca [36] using the CD-Bonn and Doleschall INOY04 potentials and the results of Viviani [42] using a potential derived from chiral potential theory (ChPT). The splitting δ is defined in the text.

phase-shifts and also better to reproduce the A_{y0} measurements of Ref. [4]. Here, this potential improves the description of A_{0y} somewhat, but has little effect on A_{xx} and A_{yy} . Considering the phase shifts, this model better describes 3P_0 and produces a P -wave splitting closer to the experimental results.

The addition of explicit phenomenological $3N$ forces in theoretical calculations has traditionally not provided full agreement between experiment and theory for $p + {}^3\text{He}$ observables, especially for A_{y0} . New results from Viviani [41,42] using $2N$ [39] and $3N$ [43] interactions derived from chiral perturbation theory at N3LO and N2LO, respectively, are shown in Fig. 10. The calculations, made using the Kohn variational principle and the hyperspherical harmonic technique, are compared with both the present A_{0y} and A_{yy} results and the A_{y0} results from Ref. [4] at 4 MeV. A satisfying reduction of A_y puzzle differences was obtained using this effective-field-theory version of the $3N$ interaction, corresponding to the improved agreement with the triplet P -wave phase shifts shown in Fig. 9. Better agreement for the $\epsilon(1^-)$ mixing parameter is also evident. Though theoretical

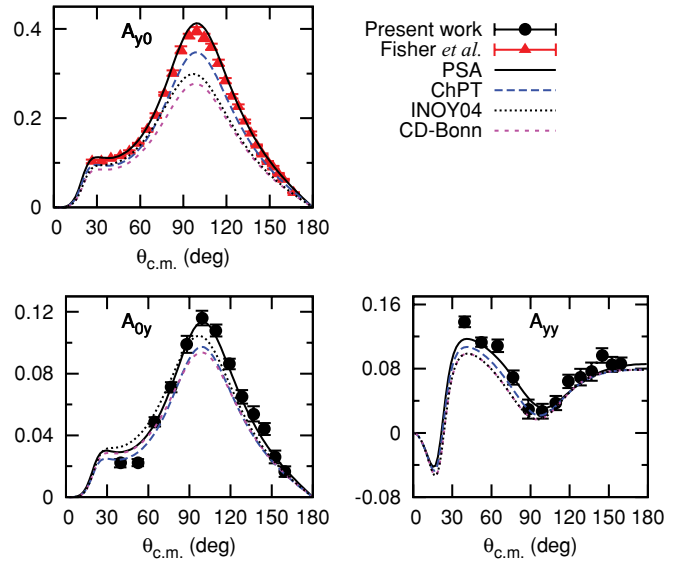


FIG. 10. (Color online) Comparison of the present observables A_{0y} and A_{yy} measured at 4 MeV, along with the A_{y0} measurements of Fisher *et al.* [4], with the theoretical results of Viviani [42] using a potential derived from chiral potential theory (ChPT). The results of Deltuva and Fonseca [36] using the CD-Bonn and INOY04 potentials are also shown.

agreement with experimental results is still not complete, Machleidt [44] has suggested that sizable one-loop $3N$ force diagrams exist at N4LO of the Δ -less chiral theory, or at N3LO when a phenomenological Δ is included, and that their addition may ultimately explain the remaining differences.

V. CONCLUSIONS

In this article we have presented new measurements of A_{0y} , A_{xx} , and A_{yy} for $p + {}^3\text{He}$ elastic scattering between 2 and 6 MeV proton energy. The target analyzing power measurements represent an improvement in accuracy over previous results, while the spin-correlation measurements include the lowest-energy data to date.

These new measurements were included in a global phase-shift analysis and new phase shifts were extracted. These additional data remove the ambiguity reported in Ref. [6]. Though discontinuities in the energy dependence of the D - and F -wave phase shifts were present, a single global solution was obtained by requiring that all phases be continuous over the energy range of the global database.

Recent theoretical calculations [36] using realistic $2N$ potentials underpredict the present A_{0y} results by 10%–20%, which is similar to but smaller than the previously observed 40% underprediction of A_{y0} [4,36]. The spin-correlation coefficients A_{xx} and A_{yy} are better described, though small underpredictions are observed at forward angles, and qualitatively different trends are observed at 2.25 MeV. The S -wave phase shifts agree well, but 1P_1 , 3P_0 , and $\epsilon(1^-)$ differ, and the theoretical triplet P -wave splitting is too small.

The INOY04 potential [40], which includes a phenomenological $3N$ force, improves the description of A_{0y} and 3P_0 and

increases the P -wave splitting. Calculations by Viviani [41] of $p + {}^3\text{He}$ elastic scattering observables at low energies using chiral $2N$ and $3N$ potentials show closer agreement with A_{y0} .

ACKNOWLEDGMENTS

The authors gratefully acknowledge continuing theoretical support for this work from M. Viviani (Pisa) and A. Deltuva and A. Fonseca (Lisbon). We thank E. George for making

available to us the energy-dependent $p + {}^3\text{He}$ phase-shift analysis code used previously, and we thank J. Dunham and B. Carlin whose continuing technical support throughout the project was essential to its successful completion. Additionally, we thank M. Boswell, C. Angell, and J. Newton for assistance with data taking and R. Prior for supplying the $p + {}^4\text{He}$ phase-shift code. Financial support from the US Department of Energy Office of Nuclear Physics under Grant DE-FG02-97ER4041 is also gratefully acknowledged.

-
- [1] J. Carlson and R. Schiavilla, *Rev. Mod. Phys.* **70**, 743 (1998).
 [2] D. R. Tilley, H. R. Weller, and G. M. Hale, *Nucl. Phys. A* **541**, 1 (1992).
 [3] W. Glöckle, H. Witała, D. Huber, H. Kamada, and J. Golak, *Phys. Rep.* **274**, 107 (1996).
 [4] B. M. Fisher, C. R. Brune, H. J. Karwowski, D. S. Leonard, and E. J. Ludwig, *Phys. Rev. C* **74**, 034001 (2006).
 [5] A. Kievsky, M. Viviani, L. Girlanda, and L. E. Marcucci, *Phys. Rev. C* **81**, 044003 (2010).
 [6] E. A. George and L. D. Knutson, *Phys. Rev. C* **67**, 027001 (2003).
 [7] T. Katabuchi, S. Buscemi, J. M. Cesaratto, T. B. Clegg, T. V. Daniels, M. Fassler, R. B. Neufeld, and S. Kadlecik, *Rev. Sci. Instrum.* **76**, 033503 (2005).
 [8] U. Rohrer, P. Huber, Ch. Leemann, and H. Schieck, *Helv. Phys. Acta* **41**, 436 (1968).
 [9] S. D. Baker, D. H. McSherry, and D. O. Findley, *Phys. Rev.* **178**, 1616 (1969).
 [10] D. M. Hardy, S. D. Baker, and W. R. Boykin, *Nucl. Instrum. Methods* **98**, 141 (1971).
 [11] C. Leemann, H. Bürgisser, P. Huber, U. Rohrer, H. Schieck, and F. Seiler, *Helv. Phys. Acta* **44**, 141 (1971).
 [12] R. G. Milner, R. D. McKeown, and C. E. Woodward, *Nucl. Phys. A* **497**, 495c (1989).
 [13] M. T. Alley and L. D. Knutson, *Phys. Rev. C* **48**, 1890 (1993).
 [14] P. L. Anthony *et al.*, *Phys. Rev. D* **54**, 6620 (1996).
 [15] K. Kramer *et al.*, *Nucl. Instrum. Methods A* **582**, 318 (2007).
 [16] Varian Inc. [<http://www.varianinc.com>].
 [17] E. Babcock, I. Nelson, S. Kadlecik, B. Driehuys, L. W. Anderson, F. W. Hersman, and T. G. Walker, *Phys. Rev. Lett.* **91**, 123003 (2003).
 [18] A. Couture, T. V. Daniels, C. W. Arnold, and T. B. Clegg, *Bull. Am. Phys. Soc.* **51**, 20 (2006) [<http://meetings.aps.org/Meeting/SES06/Event/55437>].
 [19] B. Chann, E. Babcock, L. W. Anderson, T. G. Walker, W. C. Chen, T. B. Smith, A. K. Thompson, and T. R. Gentile, *J. Appl. Phys.* **94**, 6908 (2003).
 [20] C. W. Arnold, T. V. Daniels, A. H. Couture, and T. B. Clegg, *Bull. Am. Phys. Soc.* **51**, 20 (2006) [<http://meetings.aps.org/Meeting/SES06/Event/55436>].
 [21] B. M. Fisher, Ph.D. thesis, University of North Carolina at Chapel Hill, 2003.
 [22] The Stopping and Range of Ions in Matter [<http://www.srim.org>], 2008.
 [23] G. G. Ohlsen and P. W. Keaton, *Nucl. Instrum. Methods* **109**, 41 (1973).
 [24] T. B. Clegg *et al.*, *Nucl. Instrum. Methods A* **357**, 200 (1995).
 [25] P. Schwandt, T. B. Clegg, and W. Haberli, *Nucl. Phys. A* **163**, 432 (1971).
 [26] G. R. Plattner and A. D. Bacher, *Phys. Lett. B* **36**, 211 (1971).
 [27] D. M. Hardy, R. J. Spiger, S. D. Baker, Y. S. Chen, and T. A. Tombrello, *Phys. Lett. B* **31**, 355 (1970).
 [28] D. M. Hardy, R. J. Spiger, S. D. Baker, Y. S. Chen, and T. A. Tombrello, *Nucl. Phys. A* **195**, 250 (1972).
 [29] G. G. Ohlsen, *Rep. Prog. Phys.* **35**, 717 (1972).
 [30] G. Szaloky and F. Seiler, *Nucl. Phys. A* **303**, 51 (1978).
 [31] E. A. George (private communication).
 [32] J. M. Blatt and L. C. Biedenharn, *Rev. Mod. Phys.* **24**, 258 (1952).
 [33] F. James, *MINUIT: Function Minimization and Error Analysis Reference Manual*, 1994, CERN [<http://wwwasdoc.web.cern.ch/wwwasdoc/minuit/minmain.html>].
 [34] M. T. Alley, Ph.D. thesis, University of Wisconsin-Madison, 1992.
 [35] M. T. Alley and L. D. Knutson, *Phys. Rev. C* **48**, 1901 (1993).
 [36] A. Deltuva and A. C. Fonseca, *Phys. Rev. Lett.* **98**, 162502 (2007).
 [37] R. Machleidt, *Phys. Rev. C* **63**, 024001 (2001).
 [38] R. B. Wiringa, V. G. J. Stoks, and R. Schiavilla, *Phys. Rev. C* **51**, 38 (1995).
 [39] D. R. Entem and R. Machleidt, *Phys. Rev. C* **68**, 041001(R) (2003).
 [40] P. Doleschall, *Phys. Rev. C* **69**, 054001 (2004).
 [41] M. Viviani, Proc. of 19th Intern. IUPAP Conf. on Few-Body Problems in Physics, Bonn, Aug. 31–Sept. 5, 2009, edited by E. Epelbaum, H.-W. Hammer, and U.-G. Meissner, EPJ Web of Conferences (2010) [http://www.epj-conferences.org/index.php?option=com_toc&url=/articles/epjconf/abs/2010/02/contents/contents.html].
 [42] M. Viviani (private communication).
 [43] V. Bernard, E. Epelbaum, H. Krebs, and Ulf-G. Meissner, *Phys. Rev. C* **77**, 064004 (2008).
 [44] R. Machleidt, in 28th International Workshop on Nuclear Theory, Rila Mountains, Bulgaria, 22–27 June 2009; arXiv:0909.2881v1.